THE RESPONSE OF THE UBAYE VALLEY (FRANCE) FOR INCIDENT *SH* AND *SV* WAVES: COMPARISON BETWEEN MEASUREMENTS AND MODELING

BY D. JONGMANS AND M. CAMPILLO

ABSTRACT

This paper presents a detailed study of the response of an alluvial valley in the Alps (France). The structure (Ubaye Valley) was chosen 1) for its moderate dimensions (500 m wide and 65 m thick), which allow an accurate determination of the deposit characteristics, and 2) for the relatively high seismicity of the region.

The study included the deployment of five temporary seismological stations, a seismic survey of the valley for determining the dynamic properties and the geometry of the soft deposits, and 1D and 2D numerical modeling for incident *SH* and *SV* waves.

Comparisons between observed and computed amplifications show a good agreement for frequencies lower than 10 Hz and the particular direction of arrival of the input motions corresponding to the 2D case. When the earthquake sources are not located in the continuation of the line of seismometers, the spectral ratios exhibit a great variability between different groups of similar events. These observations indicate the azimuthal dependence of the site response and the need for 3D modeling.

INTRODUCTION

Strong ground motions are characterized by a great spatial variability as indicated by the uneven distribution of damage during large earthquakes. The Valparaiso earthquake of March 3, 1985 ($M_w = 8.0$) in Chile, the Michoacan earthquake of September 19, 1985 ($M_w = 8.0$) in Mexico, and the Loma Prieta earthquake of October 18, 1989 ($M_w = 7.0$) in California have dramatically shown the influence of shallow structures on the amplitude and spectral characteristics of the ground motion (Celebi, 1987; Campillo *et al.*, 1989; Bonamassa and Vidale (1991); Borcherdt and Glassmoyer, 1992). The importance of soft surface layers for the evaluation of the seismic hazard is now widely accepted in the engineering and seismological communities. Some review papers covering observed amplification effects and methods for site response prediction were presented by Sanchez-Sesma (1987) and Aki (1988).

While the qualitative observations of site effects are numerous, the quantitative evaluations of the amplification of a well-defined 2D structure remain rare. A comparison between measurements and theoretical predictions was made by Bard and Tucker (1987) for the Chusal Valley, Garm, USSR. They found a general good agreement between observed and predicted motions.

In this paper we study the dynamic response of a small valley of about 500 m wide. For this purpose an experiment associating a seismic survey with the operation of a temporary seismological array was carried out.

The location of the experiment was chosen in the Ubaye Valley (French Alps) for three main reasons: the level of seismicity of the region, the absence of seismic noise due to human activity, and the topography near the site of Maljasset that suggests the valley may be considered two-dimensional.

GEOLOGICAL AND SEISMOLOGICAL SETTING

The site of Maljasset along the Ubaye River is located in the French Alps close to the Italian border (see Figure 1). This zone belongs to the Briançonnais arc, which is an internal unit of the western Alps. It consists of a siliceous basement (Permo-Carboniferous age) overlain by calcareous cover (Mesozoic and Eocene).

This region has one of the highest rates of seismicity in the French Alps. Several historical earthquakes have been reported. The last damaging earthquake was felt in 1959 (magnitude 5.3). During a seismicity study in this area, Frechet and Pavoni (1979) recorded several swarms with a total number of 1800 earthquakes in two months. During our experiment, the earthquakes were much less numerous (about 25). Presently, permanent networks are operating in the region (SISMALP and LDG networks) and have allowed the location of half of the events. The characteristics of these earthquakes will be discussed in the following.

SEISMIC EXPLORATION OF THE SITE

Our investigation campaign has two goals: to determine the geometry of the valley at depth and to measure P- and S-wave velocities and quality factors in each geological unit.

The substratum corresponds to Cretaceous limestone that outcrops on the northern edge. The filling of the valley is a mixture of alluvium and moraines.

The exploration of the site began with 17 reversed refraction profiles (P wave) whose lengths range between 45 and 360 m. The seismic sources used were sledge hammer for the shortest profiles and explosives for long distances. We also performed a series of four S-wave refraction profiles with a maximum source receiver distance of 180 m. The horizontal impact of a hammer on to one side of a loaded plank was used as a shear wave source. The locations of the different seismic profiles are shown in Figure 2. During this experiment we increased the recording duration in order to get the surface waves. We used the Rayleigh wave dispersion to infer the distribution of S-wave velocity at depth by an iterative inversion (Herrmann, 1985). The results obtained with this approach are in good agreement with those inferred from S-wave refraction profiles as shown in Jongmans et al. (1990).

A high resolution reflection profile was also carried out in order to map the bedrock in the central part of the valley at a depth of about 65 m.

The results obtained indicate that the bedrock consists of unweathered limestone with P-wave velocity varying from 4500 to 5500 m/sec (V_s = 2100 to 2400 m/sec). The maximum thickness of the deposits is about 65 m. The inner structure of the valley contains three different units, as shown in Figure 3 where we present its geometry with the values of P and S waves respectively. The superficial layer (referred to as Formation 1) is made up of recent alluvium from the Ubaye River and of colluvium from the relatively steep shoulders of the valley. The corresponding wave velocities are low and present rapid lateral variations (V_s = 150 to 350 m/sec). The deeper deposits can be separated into two distinct units with different wave velocities. Formation 2 lies just beneath Formation 1 and extends throughout the structure. The S-wave velocity usually ranges from 500 to 750 m/sec. In the deeper part of the valley, the bottom of the deposits (Formation 3) reaches higher velocities (V_s = 1100 m/sec), which may correspond to consolidated moraines.
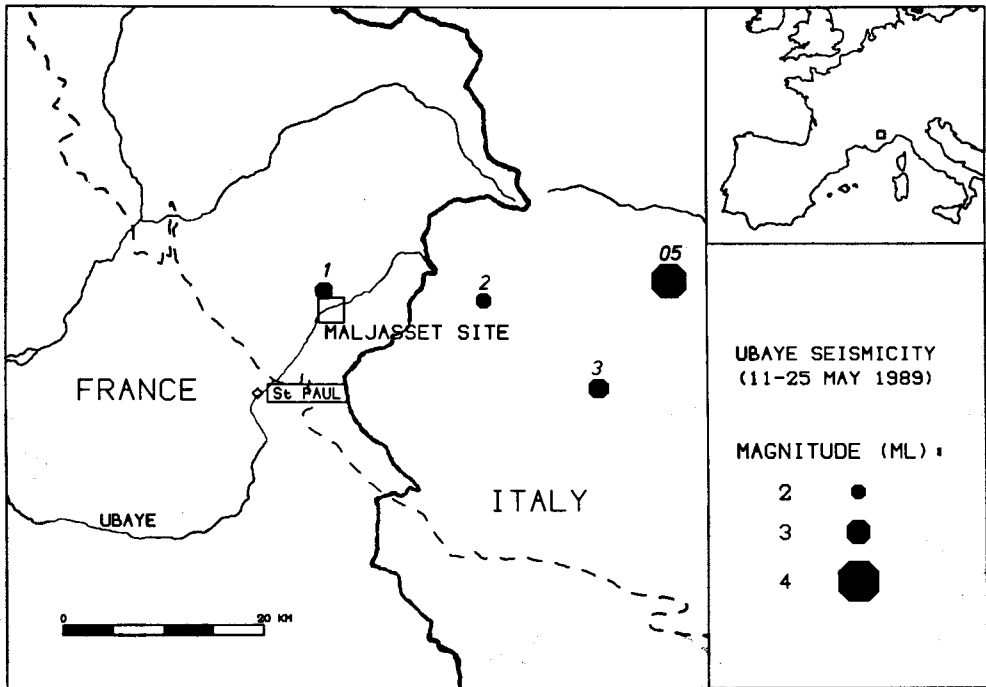
FIG. 1. Map of the Ubaye Valley showing the Maljasset site (square symbol) and the epicenter locations (numbered 1, 2, 3, and 05) of the different earthquake groups. The dashed line represents the Pennine front.

Besides the geometry of the interfaces and the different wave velocities, we need two other important parameters to compute the valley response: the quality factors Q_s and Q_p. The problem we address is to determine soil Q values from seismic survey data.

Among the various methods proposed to compute Q, the following ones were previously tested (Jongmans, 1990) with synthetic seismograms: the rise time method, the surface wave attenuation study (SWAS), and the spectral ratio method. From this work, it appeared that the first two techniques are able to deduce correct Q values in a horizontal layered medium. On the other hand, the spectral ratio method, applied to refraction data, was found less reliable, owing to the difficulty of obtaining a signal part free from interference in usual seismograms. For this reason, this approach was not used and only the two others methods are discussed further.

Real attenuation measurements remain a crucial problem, mainly because of the question of the frequency dependence of Q. A lot of literature is devoted to this difficult subject (see, for a review, Johnston and Toksöz, 1981). In geophysical prospecting and earthquake engineering, the usual assumption, based on a large amount of data, is that Q is independent of frequency. However, some experiments, both in the field (Meissner and Theilen, 1986) and in the laboratory (Johnston and Toksöz, 1981), show clear variations of Q with the frequency. It is well known at another scale that scattering in the lithosphere may yield to such a frequency dependence (Aki, 1982). The same phenomenon occurring at a scale from a few meters to a few hundred meters could explain

▲   Seismological station

◄──────►   Refraction profile
            (Direct and reverse shots)

▬▬▬▬   Reflection survey

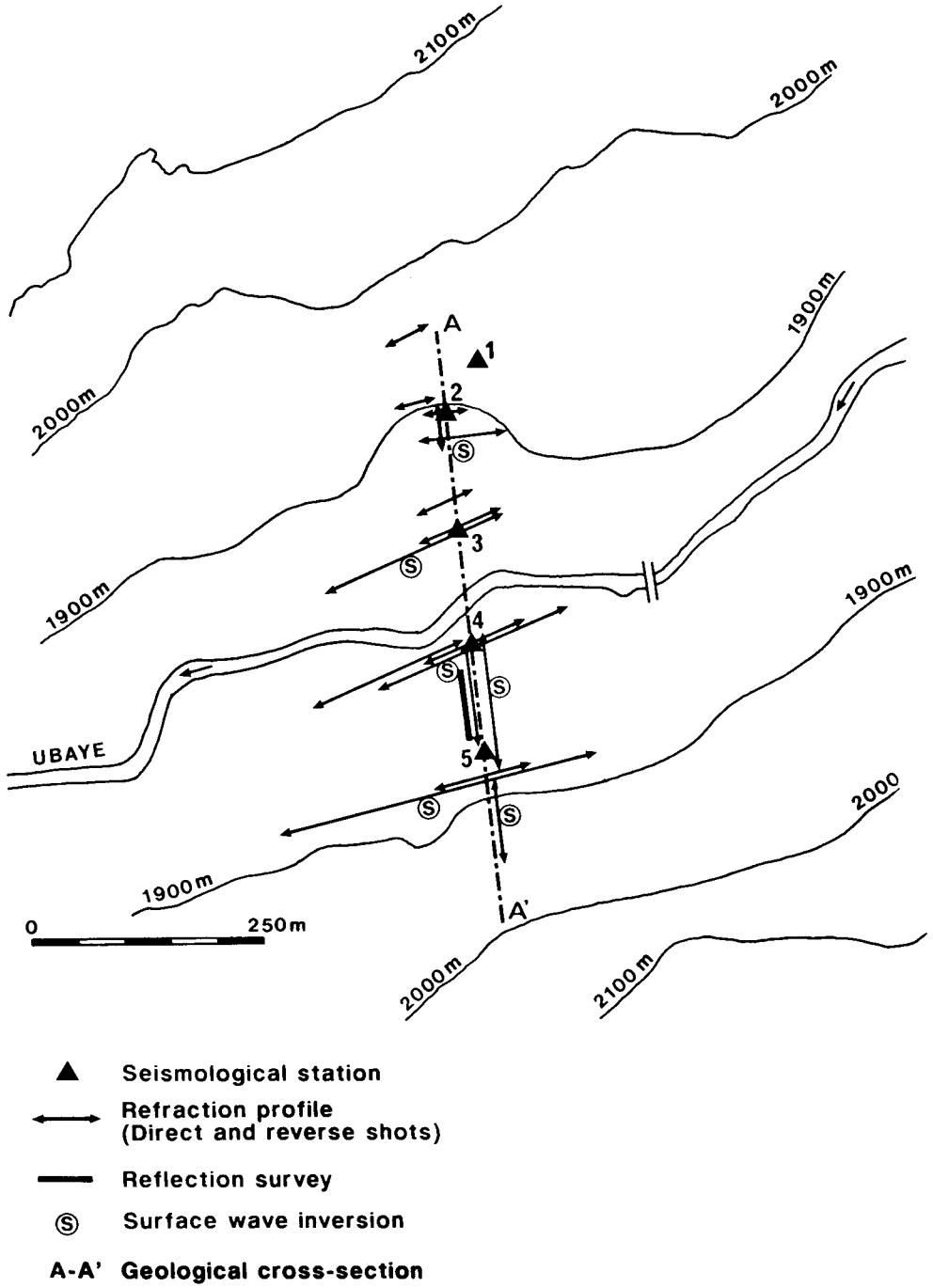Ⓢ   Surface wave inversion

A-A' Geological cross-section

FIG. 2. Map view of the experiment site with the locations of the seismic surveys.
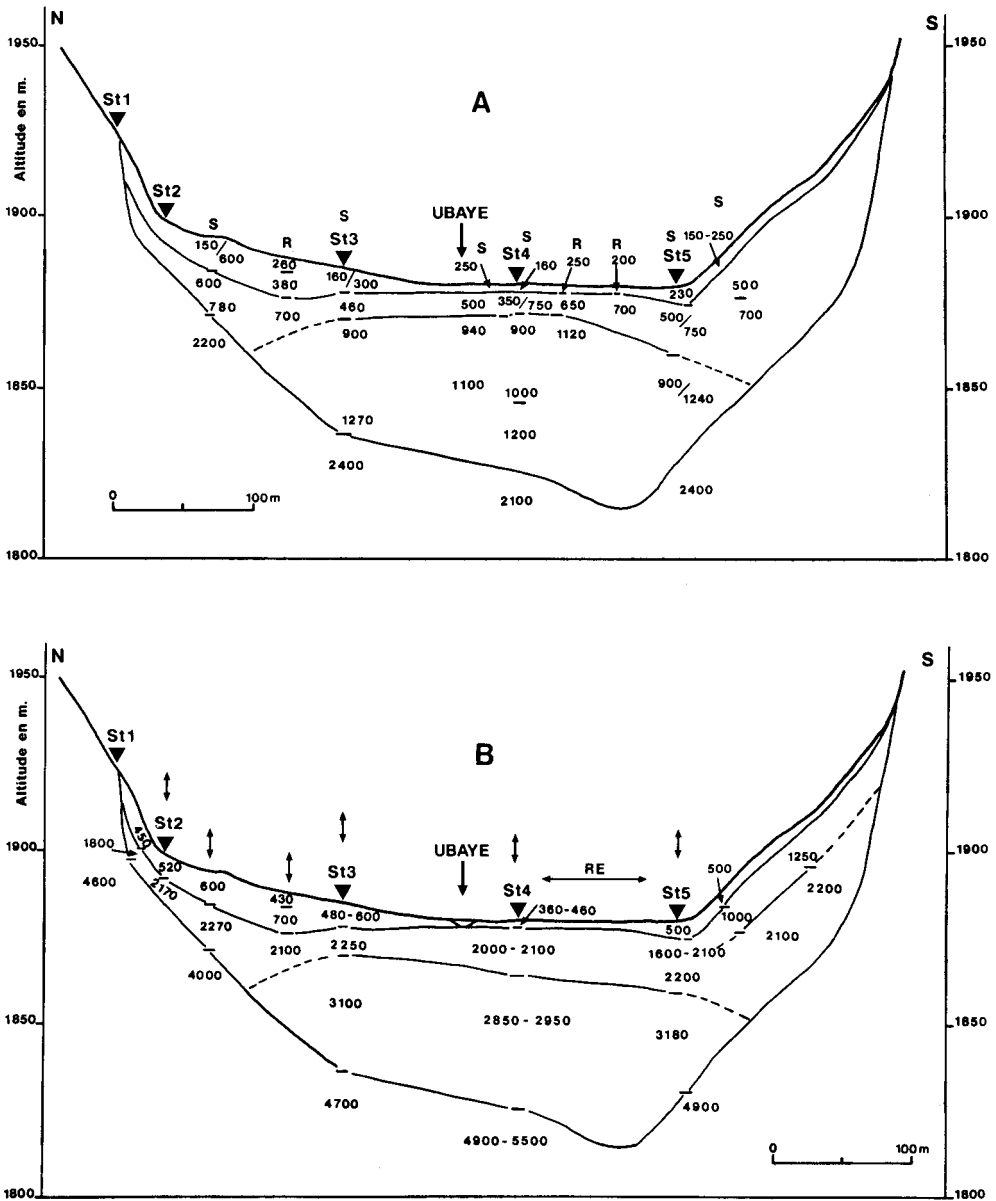
FIG. 3. Cross sections along the profile AA' (Fig. 2) perpendicular to the valley axis. (*A*) *S*-wave velocity values deduced from *SH* refraction profiles (*R*) and surface wave inversion (*S*). The notation 500/750 means that the velocity ranges from 500 to 750 m/sec from the top to the bottom. (*B*) *P*-wave velocity values inferred from refraction tests.

the Q variations in surficial layers. Our aim is, however, to determine realistic values of Q for earthquake simulations and attenuation measurements will be carried out in different frequency ranges.

The Rise Time Method

The rise time method is based on the broadening of the first pulse resulting from the attenuation of the high-frequency components. The rise time τ was

defined by Gladwin and Stacey (1974) as the ratio of the maximum peak amplitude to the maximum slope of the first quarter-cycle of the pulse. From their experiments, they proposed the following relationship:

$$\tau = \tau_0 + \frac{C}{Q}t \tag{1}$$

where τ and τ_0 are the rise times at the measurement point and at the source, t is the traveltime and C is a fixed constant.

As pointed out by Blair and Spathis (1984), the factor C is source dependent and has to be estimated for each data set. The way to overcome this difficulty is to simulate the wave propagation in an attenuating medium (with a constant Q value) and to compare the results to the data.

This method has been applied to the S-wave refraction data recorded in the Ubaye Valley. The frequency range of the signal is between 25 and 60 Hz. Beyond a distance of 1.2 wavelength, the relation between τ and t is almost linear and the rise time method leads to a Q_s value of 5.4. At close distance from the source, the pulse shape is mainly controlled by the near field terms and the onset of surface waves (Jongmans, 1991).

Surface Wave Attenuation Study (SWAS)

The SWAS method consists in computing the frequency-dependent attenuation factor of the surface wave amplitude (Herrmann and Mitchell, 1975). These data are then inverted in order to obtain a vertical Q_s profile.

From the field seismograms, plotted on Figure 4, we have computed the attenuation curve. The frequency range of the signal varies between 9 and 16 Hz. The inversion of the attenuation data leads to the $1/Q_s$ profile as a function of depth (Figure 4).

Q_s Values

All the results of Q_s determinations are given in Table 1. In a general way, Q_s values obtained at high frequency (25 to 60 Hz) with the rise time method are about 5 to 6 in Formations 2 and 3. They are systematically lower than those inferred from Rayleigh waves in a lower frequency range (9 to 16 Hz). These results, also observed on other sites by Jongmans (1990), may indicate a frequency dependence of Q in surficial materials.

As we will see later, higher Q_s values (10 to 20) are far more consistent with the experimental valley response.

SEISMOLOGICAL STUDY

During the month of May 1989, a temporary network of five stations was installed in the site of Maljasset (see Figure 2 for their locations). We used identical digital stations equipped with three-component seismometers with natural frequency of one Hz. Station 1 is located on hard rock and is used as a reference to evaluate the incoming wave field. The other stations were set up at equal intervals across the valley. Since the site is at an altitude of 1900 m, technical problems arose due to the large variations of temperature.

In order to study the experimental site response, the 12 events recorded by at least three stations were selected. Their characteristics are given in Table 2.
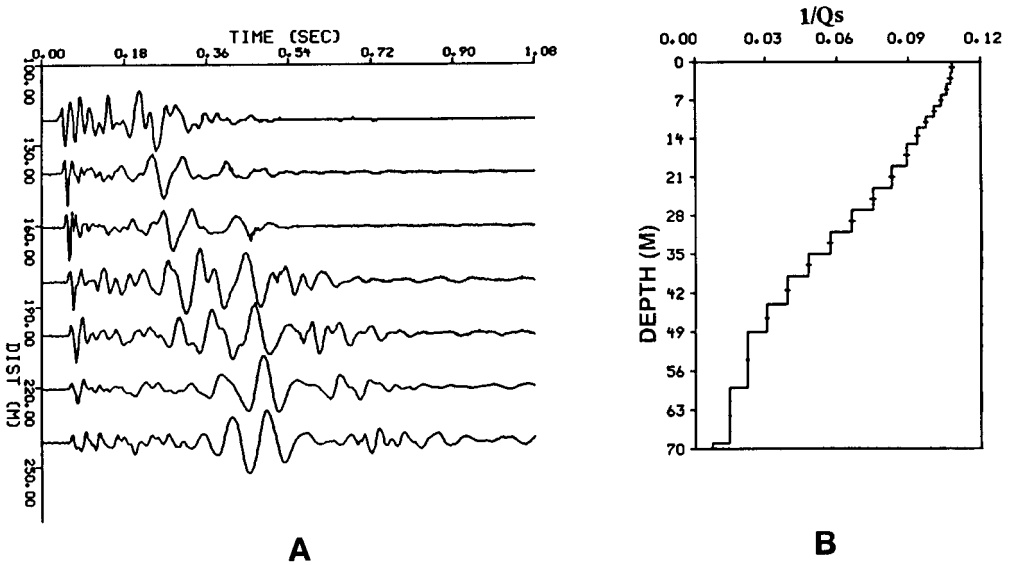
FIG. 4. (*A*) Field seismograms (vertical component) showing prominent Rayleigh waves. (*B*) Q_s profile as a function of depth.

TABLE 1

Q_s AND Q_p VALUES INFERRED FROM IN SITU TESTS

Unit	Method	Q_p	Q_s	Frequency (Hz)	
				P	S
2	Rise time	5.5–7.5	5–6	50–90	40
	Surface wave	—	10	—	9–16
3	Rise time	11	5–6	60–100	30–50
	Surface wave	—	20	—	9–16

TABLE 2

LIST OF THE EARTHQUAKES WITH THEIR MAIN CHARACTERISTICS

Number	Date (d/m/y)	Hour	M_L	t_s-t_p (sec)	Epicentral Distance (km)	Depth (km)
5	12/05/89	11h27m	3.6	3.79	34.3 ± 2	9 ± 4
7	17/05/89	03h09m	2.3	0.46	6.9 ± 2	0 ± 2
10	17/05/89	06h04m	0.5	0.55	10 ± 26	0 ± 8
11	17/05/89	07h59m	2.5	0.54	6 ± 3	3 ± 2
12	17/05/89	08h12m	1.8	0.54	3.2 ± 1	2.8 ± 0.5
13	17/05/89	08h14m	< 2	0.52	—	—
15	18/05/89	12h16m	< 2	2.30	4.5 ± 3	16 ± 1
16	18/05/89	13h03m	1.9	2.18	14.4 ± 2	9 ± 1
19	22/05/89	20h05m	2.3	2.00	18.5 ± 2	7 ± 2
22	25/05/89	13h51m	2.4	3.30	27.3 ± 1	2 ± 2
23	25/05/89	18h58m	2.7	3.24	26.1 ± 1	7 ± 2
24	25/05/89	22h00m	2.7	3.50	36.5 ± 2	3 ± 3

Due to the lack of data there is no reliable focal mechanism available. We organized this set of earthquakes into three groups based on location. In order to verify that this division is accurate, the spectra of the horizontal motions (S waves) at the hard rock station are compared for the different events and the analogy of the shape of the spectra is checked for the different groups of earthquakes.

The earthquakes are subdivided as follows:

Group 1: events 7, 10, 11, 12, and 13

Group 2: events 15, 16, and 19

Group 3: events 22, 23, and 24.

The epicenter locations of the main event of each group are shown in Figure 1.

Event 05 is different from the others both by its magnitude (3.6) and its location. Group 1 consists of local shallow earthquakes that occurred in the north of the site in the direction of the alignment of the five stations. The epicentral distances are less than 10 km. Groups 2 and 3 correspond to earthquakes located at distances larger than 15 km and 25 km, respectively.

SITE RESPONSE

We present in Figure 5 an idealized seismic section of the valley with the N–S horizontal motions observed from event 12 at the five stations. The seismograms are plotted at the same scale and illustrate the amplification of the ground motion at location over the alluvium with respect to hard rock site (station 1). The motion duration also appears to be larger on all the stations located on soft sediments.

Figure 6A presents the three-component records of earthquake 05 at stations 1 to 3. The duration of the seismograms is 25 sec. An amplification effect appears clearly on the three components of the signals recorded at stations 2 and 3. In order to visualize the frequency effect the E–W horizontal seismograms are filtered in the frequency bandwidths 1 to 5 Hz and 5 to 25 Hz (Figure 6B).

In the frequency range between 5 and 25 Hz, the records at stations 2 and 3 show large amplification with respect to station 1. On the contrary, in the low-frequency range, no significant difference can be found between the seismograms at stations 1 and 2, while station 3 exhibits a small amplification effect. In the same time the envelope of the low-frequency seismograms changes significantly between station 2 and station 3. The duration of the signal is larger at station 3 with the appearance of a slowly decaying coda. This increase of duration at station 3 can be seen also in the high-frequency range (5 to 25 Hz) for this event.

It is noteworthy that, for records of event 12 (Figure 5), the increase of duration is much smaller and does not exceed 1 sec. This point suggests that the response of the valley is qualitatively different for these two events.

In order to quantify the amplification effect, the signals were windowed to extract S waves and we computed the spectral ratios between the signals observed at sites in the valley and the signal recorded at the reference hard rock station. The spectra were smoothed before the spectral ratios were calculated. Figure 7 presents the spectral ratios of the two horizontal components recorded for the events of Group 1. The mean spectral ratio is also drawn with dashed
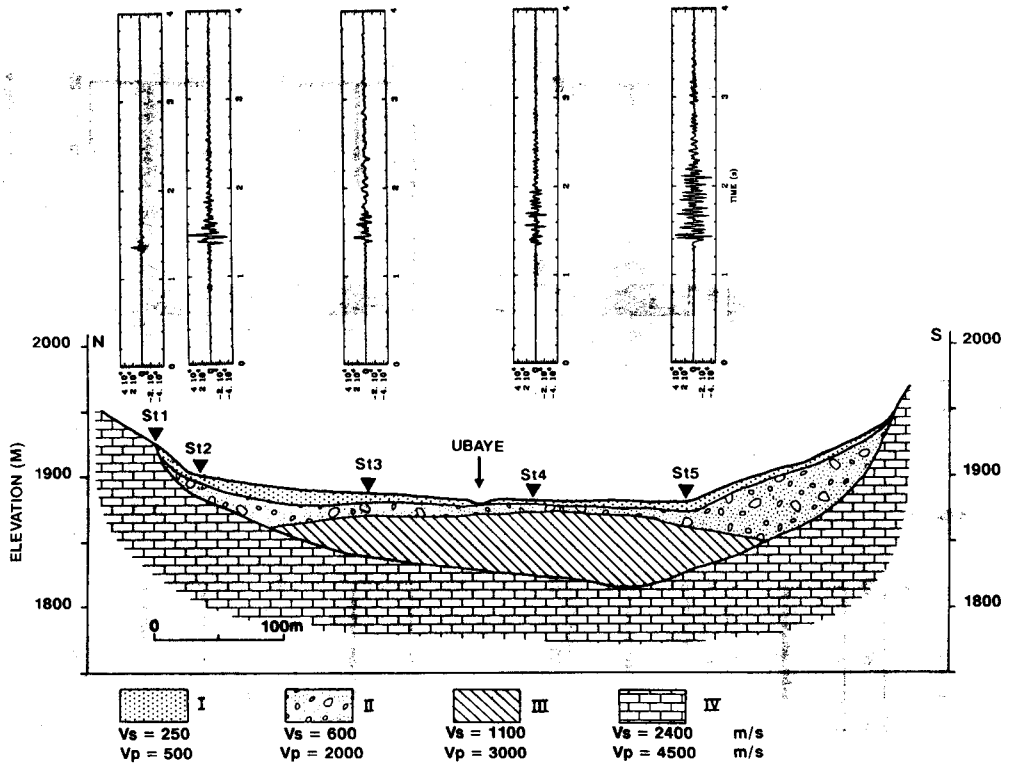
FIG. 5. Idealized seismic section used for 2D modeling and N–S horizontal seismograms recorded for an earthquake of Group 1 at the different stations.

lines. At each station the ratios exhibit similar features in most of the cases except at site 5 where discrepancies appear above 20 Hz. The existence of spectral bands of amplification centered on the same values of frequency is characteristic of the response of the soft deposits.

We have just shown the relative stability of the spectral ratios for earthquakes of a given group but this property disappears when comparing records for events from different groups. This is illustrated with Figure 8 which presents the mean values of the spectral ratio computed for each group of earthquakes. We have plotted separately the curves corresponding to the earthquake 05, which has a magnitude and an epicentral distance different from the other events. In some cases we have also computed the spectral ratio for the seismic noise. The clear difference between the results obtained from earthquakes and from noise is probably due to the part played by the river as a source of local noise. The spectral ratios computed for the earthquake groups show in most cases differences that prevent the indentification of a common response at the sites.

From the examination of these figures, we can draw the following conclusions:

1. the spectral amplifications vary from one station to another both in terms of maximum value and of shape of the response curve,

2. the values of amplification and the position of the peaks change from one horizontal component to the other, and
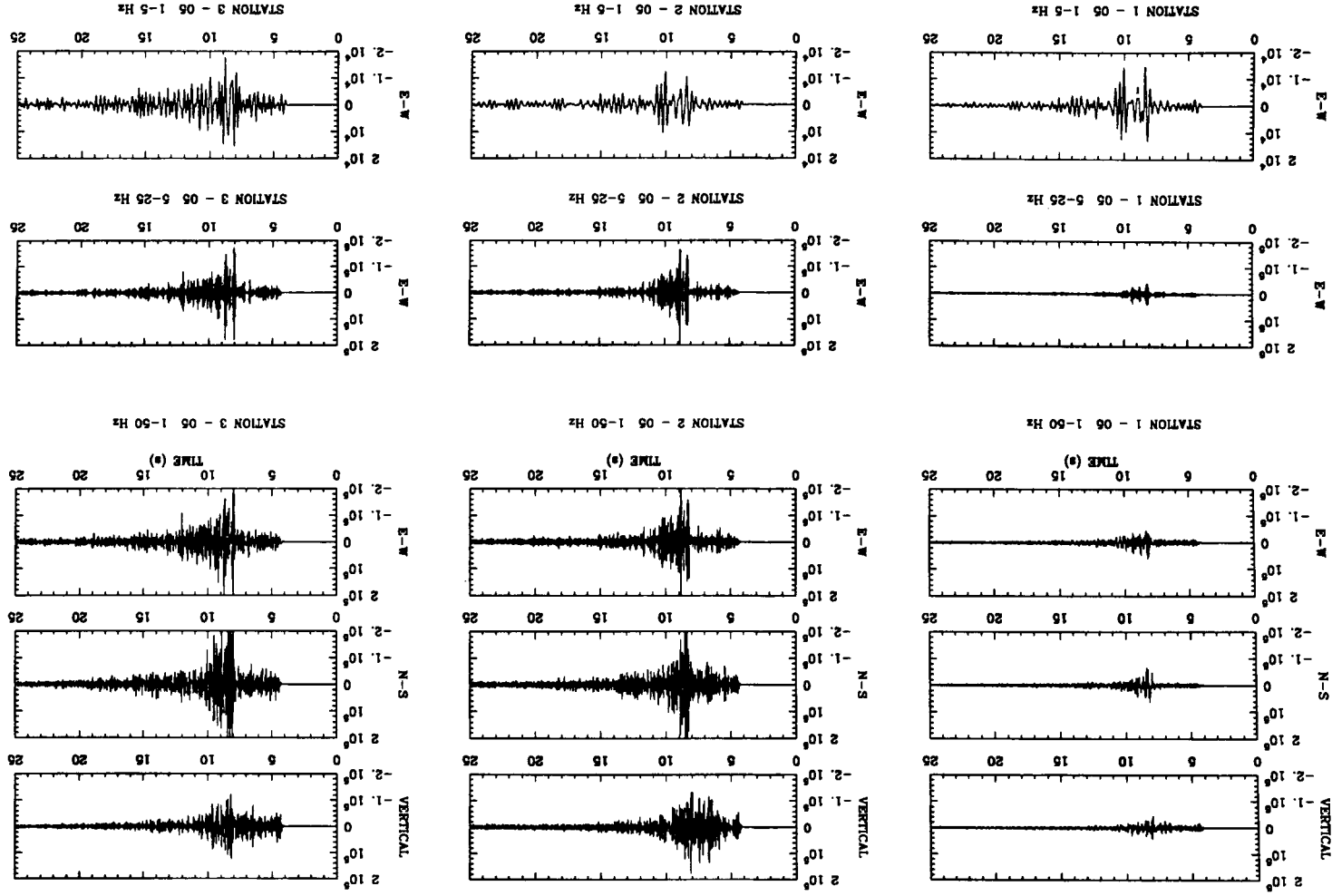
FIG. 6. Seismograms recorded during earthquake 5 at stations 1, 2, and 3. (Top) Three component records filtered in the 1 to 50 Hz frequency bandwidth. (Bottom) Records filtered in the 5 to 25 Hz and the 1 to 5 Hz frequency bandwidth, respectively.
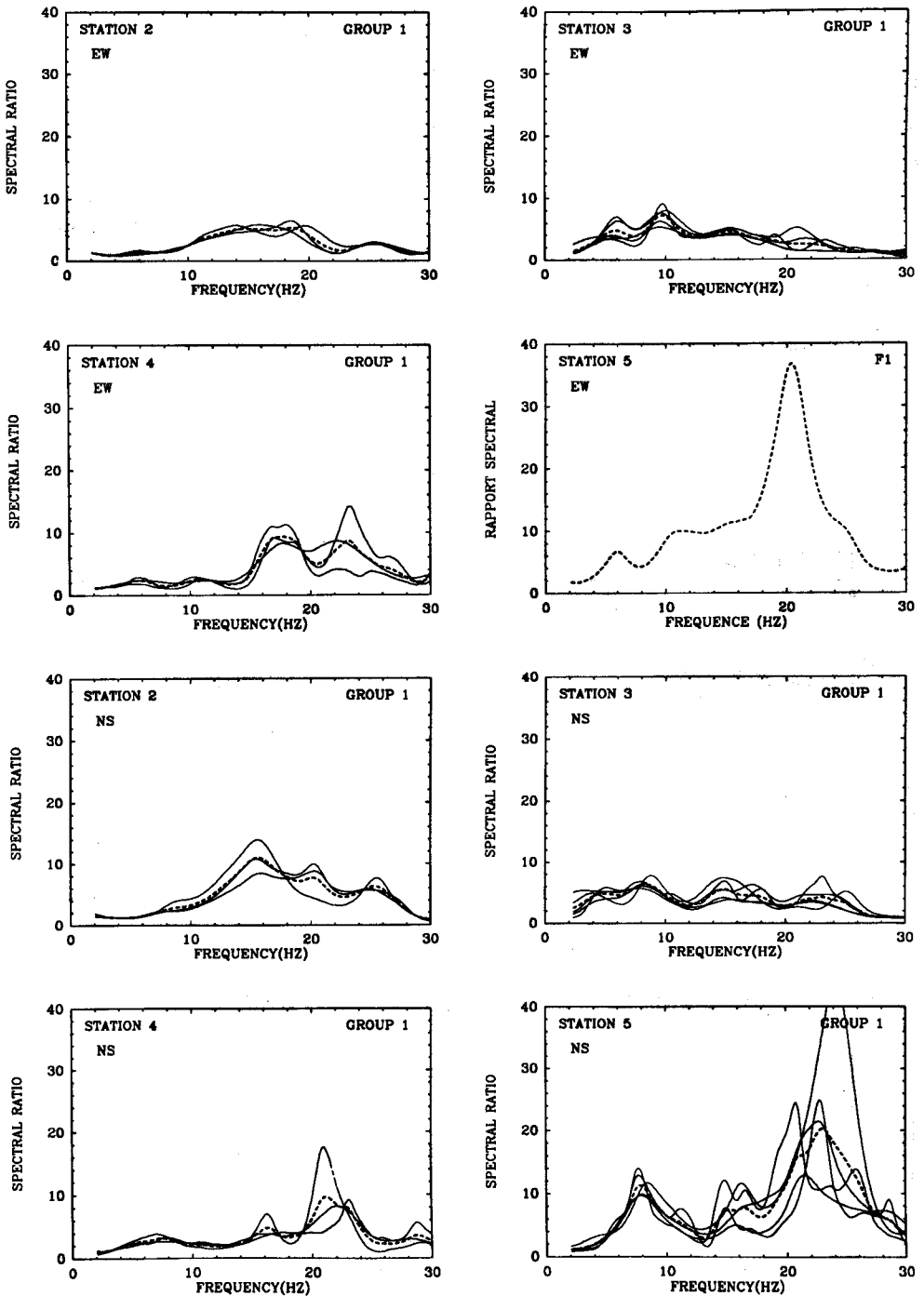
FIG. 7. Spectral ratios for the events of Group 1 (E–W and N–S components). The mean value is plotted as a dashed line.
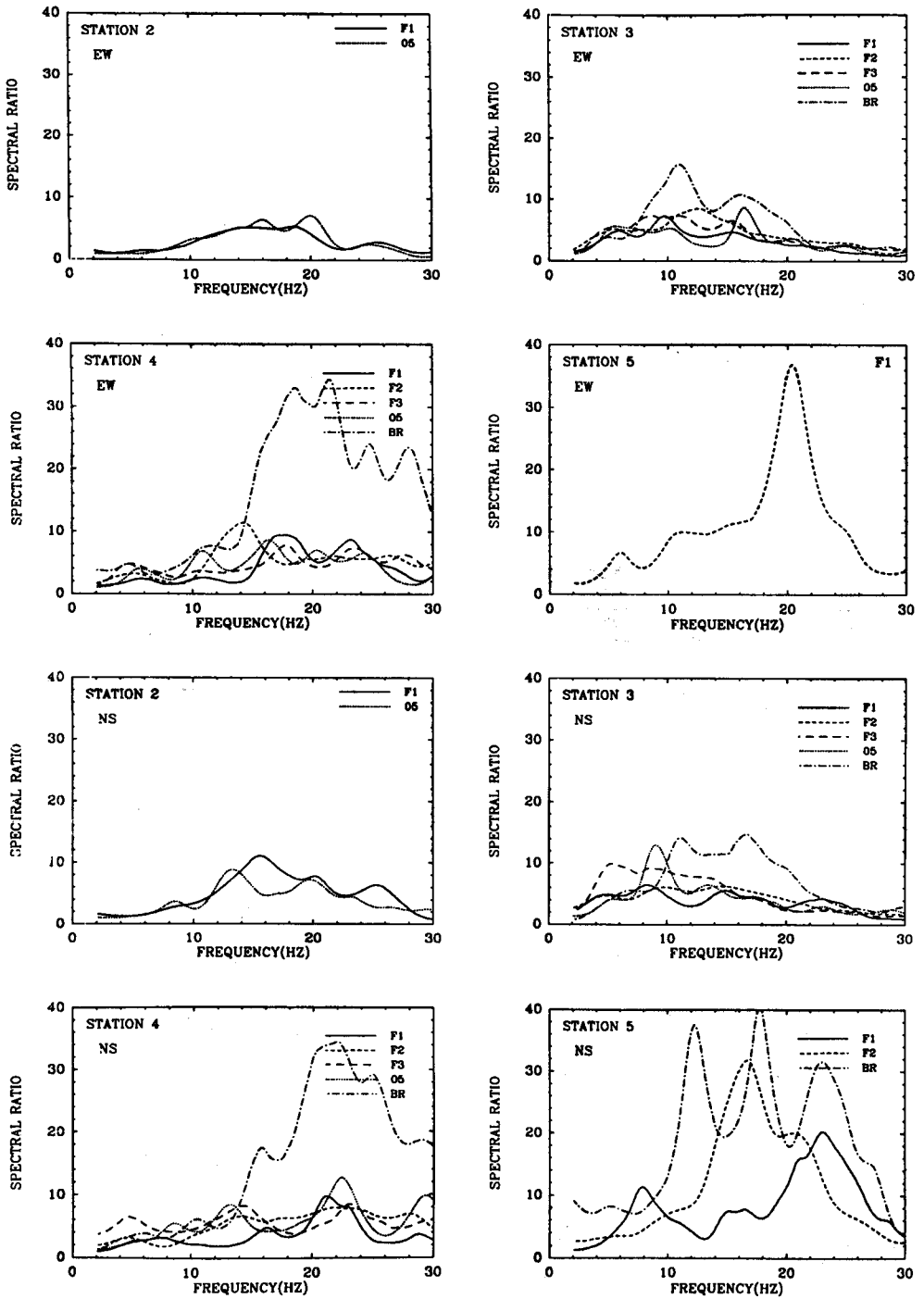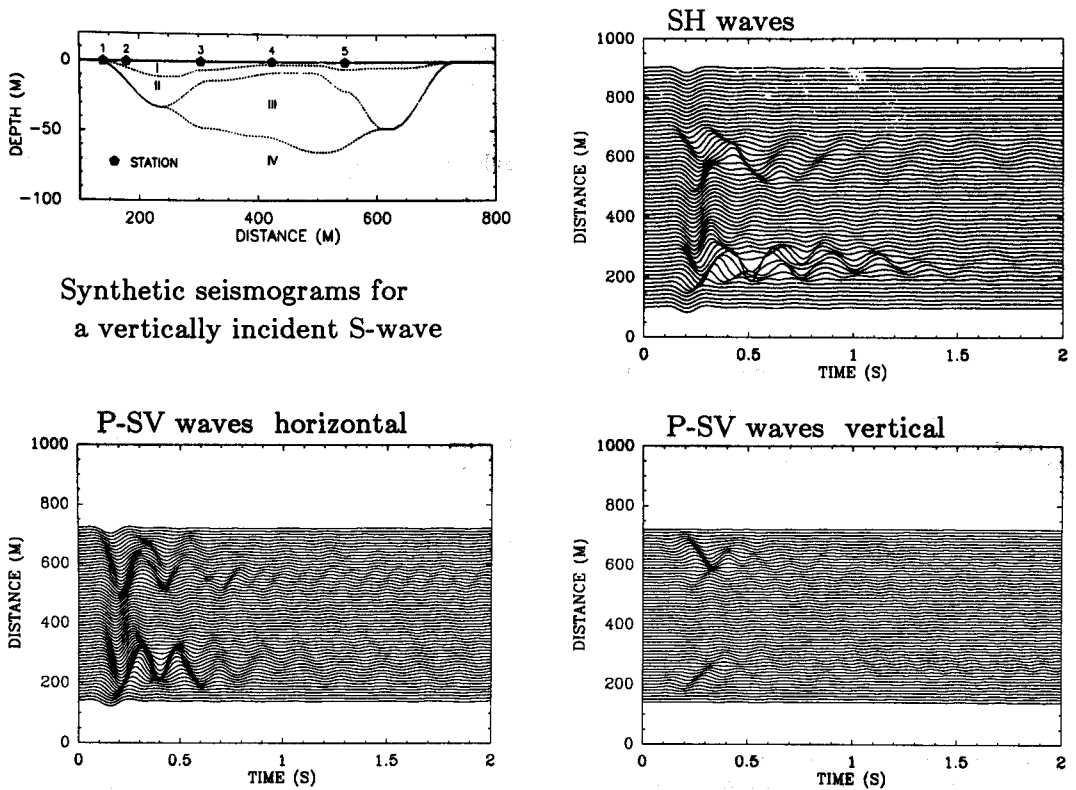
FIG. 8. Comparison between the mean spectral ratios computed for the different groups of earthquakes. The curves corresponding to Groups 1 to 3 are labeled F1 to F3. The dashed line (*BR*) is the mean ratio obtained from the seismic noise.

FIG. 9. 2D model used in the numerical simulations and synthetic seismograms computed for vertical incident waves (Ricker 5 Hz).

3. the spectral ratios are also dependent on the group of earthquakes considered.

In order to further understand the amplification effects and their variability, these observations are compared with theoretical predictions.

2D MODELING

To compute the response of the 2D structure inferred from the results of the surveying (Figure 3), we used a boundary integral equation method in a formulation described by Bouchon *et al.* (1989) and Gaffet and Bouchon (1991). This method allows the inclusion of steep interfaces and high-frequency waves. In this application, we considered frequencies in the range 0 to 25 Hz and 0 to 9 Hz for the *SH* and *P–SV* cases respectively. We constructed the model for the simulation by representing each interface with a series of branches of cosine and straight lines. It is presented in Figure 9 together with synthetic seismograms. The parameters of the medium used for the modeling are given in Table 3. The quality factors are those inferred from surface wave analysis. We assume the same values of Q for P and S waves.

The synthetic seismograms computed across the structure for vertical incident waves (a Ricker wavelet of 5 Hz) are presented in Figure 9 for the *SH* and *P–SV* cases. In both cases, it is not possible to identify waves that propagate from one edge of the valley across to the other. Thus we do not expect to observe

TABLE 3

DYNAMIC CHARACTERISTICS OF THE FORMATIONS USED FOR 2D *SH* MODELING

Formation Number	Description	V_p (m/sec)	V_s (m/sec)	Q	ρ
1	Surficial layers (alluvium, colluvium)	500	250	10	1.8
2	Alluvial deposits	2000	600	10	1.9
3	Moraines, weathered bedrock	3000	1100	20	2.0
4	Limestone	4500	2400	200	2.6

a lateral resonance of the structure. To the contrary, in each of the two zones where the layers 1 and 2 are thick, we can see reverberating waves that contribute to increase the duration of the signal and, therefore, that are the cause of some of the spectral amplification observed on some of the stations.

COMPARISON BETWEEN OBSERVED AND PREDICTED AMPLIFICATIONS

SH Modeling

We compare our computations with actual observations by selecting data that are compatible with the restrictive assumption of *SH* modeling. First, we limited our calculus to the 2D case. The shape of the valley allows this assumption in the cases when the earthquakes are aligned with the seismological stations. As mentioned before, this is the case with earthquakes of Group 1. Second, the *SH* waves appear on the E–W component of the motion.

The results are summarized in Figure 10, which presents for three stations (a) the spectral ratios computed from the E–W components of earthquake records of group 1 and (b) the theoretical spectral amplifications for 2D computations. The results of 1D computations, considering a stack of horizontal layers beneath each seismological station, are shown in the same figure for vertical *SH* incident waves. The vertical incidence hypothesis implies a strong vertical velocity gradient beneath the structure. The influence of the ray incidence angle on the results will be discussed later in the *P–SV* case.

For the three stations and for frequencies smaller than 10 Hz, the magnitude of the amplification and the shape of the spectral ratio measured from the synthetics are in global agreement with the observations.

A striking 2D effect is visible for station 2. In this case, the observed spectral ratio shows an amplification over a wide frequency band. In a 1D model the site effect would occur in a narrow band, as shown in Figure 10. On the contrary, taking into account the 2D structure, the computed spectral ratio indicates an amplification over a broad frequency band. This frequency shift results from the presence of dipping interfaces between layers 1, 2, and 3 (Figure 5). To predict the motion at station 2, it is therefore needed to consider at least a 2D model.

For station 3, our results are almost similar whatever model is considered. The prediction slightly underestimates the amplification beneath the station but gives an acceptable description of the location of the peaks of amplification. For station 4 the models and the observations are in good agreement for frequencies smaller than 10 Hz. At high frequency, the large discrepancy is probably explained by our poor knowledge of the most superficial layers that might play a prominent part in the response for frequency larger than 15 Hz. One must note that the 2D model is still too simple because each layer is
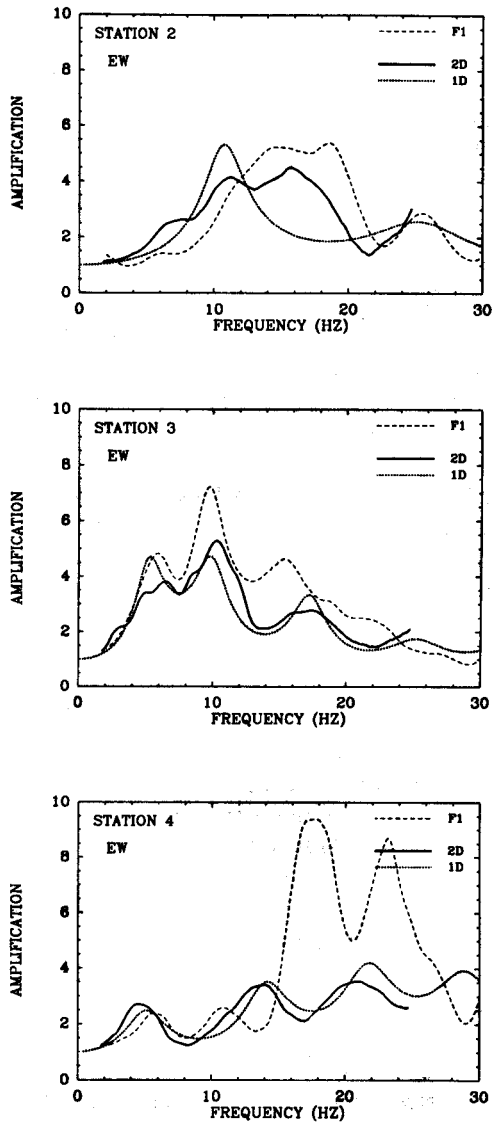
FIG. 10. Comparison between observed amplification (E–W component) for Group 1, 1D and 2D modeling (*SH* case).

defined with given wave velocity and density, while, as shown in Figure 3, our prospecting experiments indicate some lateral variations of the elastic modulus in the layer in addition to the variations of depth of the interfaces.

Even if the entire valley is not subject to resonance, 2D effects cannot be ruled out, in particular to explain local effects at the edges of the structure (station 2).

Station 5 was installed in a swampy area the characteristics of which have changed during the snow melting. Due to the large uncertainty about surficial soil properties in this area, station 5 wasn't modeled.

Another aspect which may be pointed out by the 2D-*SH* modeling of the structure is the influence of the incidence angle likely to explain some of the fluctuations of the amplification curves for the different groups of events.

Computations performed with an incidence angle of 30° show some changes in the positions of the amplification peaks as an effect of the variation of the incidence angle. On the other hand, a similar test made for the 1D model shows almost no shift in frequency. Anyway, variations of the incident angle cannot be solely invoked to explain the large variations of band amplifications observed on the spectral ratios computed for the different groups of earthquakes (Figure 8).

These results show the need for at least a 2D modeling to explain the amplification in the valley and its variability from one group of earthquakes to another. In addition, a more comprehensive examination of the data (including the nontransverse component) indicates that a 2D-*SH* modeling is not sufficient. For example, the different behavior between the two horizontal components is an important point that cannot be addressed at this stage of the simulation.

P–SV Modeling

The theoretical amplifications generated by a vertically incident *SV* plane wave are compared with the experimental spectral ratios observed for the events of Group 1 (Figure 11). In order to select the *SV* component of the motion, the spectral ratios are computed for the N–S component of the seismograms. The frequency range is between 1.5 and 9 Hz. Three different incidence angles (0°, 30°, and −30°) are considered in the computations. The theoretical results show that the influence of the incidence angle is usually small, except for station 3 where the amplification at 5 Hz is, for an angle of 30°, almost twice the one for a vertical incidence. Some amplification peak shifts are also clearly seen when the incidence angle varies.

The numerical simulations are usually able to explain the main general features observed on the experimental amplification curves. The experimental and theoretical amplifications at stations 2 and 4 are relatively small in the frequency range considered. At station 3, an amplification of about 4 is observed between 4 and 6 Hz both on theoretical and experimental results. As was discussed before, the amplification curves are very different for each group of earthquakes. This means that the satisfactory agreement found between computations and Group 1 observations disappears when considering the other groups of events. For example, the spectral ratios obtained for Group 3 are very different from the numerical results. Of course, for these earthquakes, the response cannot be reduced to a 2D problem. From a practical point of view, it is noticeable that the numerical 2D simulation would severely underestimate the amplification. These results suggest a possible azimuthal dependence of the site response. Such an azimuthal dependence has already been observed by Bonamassa and Vidale (1991) from aftershocks of the Loma Prieta earthquake.

CONCLUSIONS

The study of the Ubaye Valley has been initiated with the aim to test our capability to predict amplification effects for a given site.

The geological structure of the valley was unknown and the first step was to investigate it thoroughly with different seismic methods (refraction tests, reflection profile, and surface wave inversion). *P*- and *S*-wave velocities as well as quality factor values were inferred from these experiments.

At the same time, earthquakes have been recorded by five three-component stations located in the valley and on a rock outcrop along a profile perpendicular to the structure axis. The spectral ratios have pointed out a great variability of
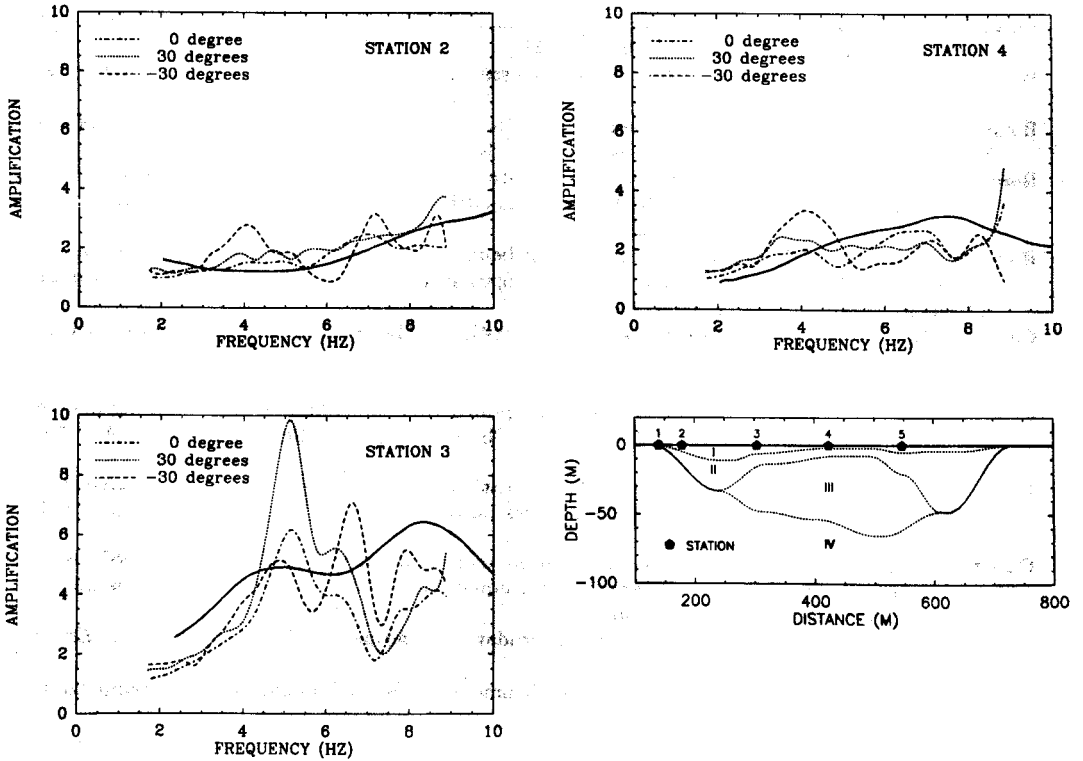
FIG. 11. Comparison between experimental amplification (N–S component) and 2D *SV* modeling for different incident angles (0°, 30°, and −30°) at stations 2, 3, and 4. The model is plot at the lower right.

the response (a) between the different stations, (b) between the two horizontal components of the same records, and (c) for different groups of earthquakes at the same station. This last observation suggests an azimuthal dependence of the site response towards the earthquake location.

On the basis of geophysical data, numerical simulations (1D and 2D modeling) were performed for the *SH* and *SV* cases. In both cases, observed and synthetic spectral ratios show a good agreement for frequencies lower than 10 Hz and for the group of events generating waves reaching the site perpendicularly to the valley (i.e., in a 2D configuration). Considering the entire set of earthquakes, the patterns appear to be more complex. If the numerical simulations are able to explain some general features of the observed spectral ratios, some important discrepancies exist between synthetic and experimental amplifications. In particular, the modeling results in an underestimation of the amplification effects. Because of the thorough investigation of the structure, we think that these discrepancies result from the limits of the 2D simulation.

To resolve this point, we will need to develop reliable tools to study 3D propagations in order to quantify the theoretical azimuthal dependence of the response.

REFERENCES

Aki, K. (1982). Scattering and attenuation, *Bull. Seism. Soc. Am.* **72**, 319–330.

Aki, K. (1988). Local site effects on strong ground motion. in *Earthquake Engineering and Soil Dynamics II—Recent Advances in Ground Motion Evaluation*, J. L. Von Thun (Editor), Geotechnical Special Publication No. 20, Am. Soc. Civil Engr., New York, 103–155.

Bard, P.-Y. and P. E. Tucker (1984). Underground and ridge site effects: a comparison of observation and theory, *Bull. Seism. Soc. Am.* **75**, 905–922.

Blair, D. B. and A. T. Spathis (1984). Seismic source influence in pulse attenuation studies, *J. Geophys. Res.* **89**, 9253–9258.

Bonamassa, O. and J. E. Vidale (1991). Directional site resonances observed from aftershocks pf the 18 October 1989 Loma Prieta Earthquake, *Bull. Seism. Soc. Am.* **81**, 1945–1958.

Borcherdt, R. and G. Glassmoyer (1992). On the characteristics of local geology and their influence on ground motions generated by the Loma Prieta earthquake in the San Francisco Bay region, California, *Bull. Seism. Soc. Am.* **82**, 603–641.

Bouchon, M., M. Campillo, and S. Gaffett (1989). A boundary integral equation–discrete wavenumber representation method to study wave propagation in multilayered media having irregular interfaces, *Geophysics* **54**, 1134–1140.

Campillo, M., J. C. Gariel, K. Aki, and F. J. Sanchez-Sesma (1989). Destructive ground motion in Mexico City: source, path, and site effects during great 1985 Michoacan earthquake, *Bull. Seism. Soc. Am.* **79**, 1718–1735.

Celebi, M. (1987). Topographical and geological amplifications determined from the strong-motion and aftershock records of the 3 March 1985 Chile earthquake, *Bull. Seism. Soc. Am.* **77**, 1147–1167.

Frechet, J. and N. Pavoni (1979). Etude de la sismicité de la zone briançonnaise entre Pelvoux et Argentera (Alpes Occidentales) à l'aide d'un réseau de stations portables, 1979, *Eclogae Geol. Helv.* **72 / 3**, 763–779.

Gaffet, S. and M. Bouchon (1991). Source location and valley shape effects on the *P–SV* near displacement field using a boundary integral equation–discrete wavenumber representation method, *Geophy. J. Int.* **106**, 341–356.

Gladwin, M. and F. Stacey (1974). Anelastic degradation of acoustic pulses in rock, *Phys. Earth Planet. Interiors* **8**, 332–336.

Herrmann, R. (1985). Computer Programs in Seismology, User's Manual, Vol. IV, Saint-Louis University, Missouri.

Herrmann, R. and B. Mitchell (1975). Statistical analysis and interpretation of surface-wave anelastic attenuation data for the stable interior of North America, *Bull. Seism. Soc. Am.* **65**, 1115–1128.

Jongmans, D. (1990). L'influence des structures géologiques sur l'amplification des ondes sismiques, *Ph.D. Thesis*, Liege University.

Jongmans, D., M. Campillo, and D. Demanet (1990). The use of surface wave inversion and seismic reflection methods for engineering applications, in *Proc. of the 6th Int. Congress of I.A.E.G.*, Amsterdam, 6–10 August, Vol. 2, 979–985.

Jongmans, D. (1991). Near source pulse propagation: application to *Q* determination, *Geophys. Prospect.* **39**, 943–952.

Johnston, D. H. and Toksöz, M. N. (1981). Seismic wave attenuation, S. E. G. Geophysics Reprint Series No. 2.

Meissner, R. and F. Theilen (1986). Experimental studies of the absorption of seismic waves, D.G.M.K.-project 254, 5–53.

Sanchez-Sesma, F. J. (1987). Site effects in strong ground motion, *Soil Dyn. Earthquake Eng.*, **6**, 124–132.

Laboratoires de Geologie de l'Ingénieur
Université de Liège
Bat. B19
4000 Liège
Belgium
  (D.J.)

Laboratoire de Géophysique Interne
  et de Tectonophysique
I.R.I.G.M.
Université Joseph Fourier
BP 53 X
F38041 Grenoble
France
  (M.C.)